J. Fluid Mech. (2000), *vol.* 416, *pp.* 197–216. Printed in the United Kingdom

Lubrication analysis and boundary integral simulations of a viscous micropump

By RICHARD F. DAY AND H. A. STONE

Division of Engineering and Applied Sciences, Harvard University, Cambridge, MA 02138, USA

(Received 15 June 1999 and in revised form 15 March 2000)

Several recent papers discuss a viscous micropump consisting of Poiseuille flow of fluid between two plates with a cylinder placed along the gap perpendicular to the flow direction (e.g. Sen, Wajerski & Gad-el-Hak 1996). If the cylinder is not centred, rotating it will generate a net flow and an additional pressure drop along the channel, due to the net tangential viscous stresses along its surface. The research reported here complements existing work by examining the lubrication limit where the gaps between the cylinder and the walls are small compared to the cylinder radius. Lubrication analysis provides analytical relations among the flow rate, torque, pressure drop and rotation rate. Optimization of the flow parameters is shown in order to determine the optimal geometry of the device, which can be used by micro-electrical-mechanical systems designers. It is also shown, for example, that a device cannot be developed that achieves maximum flow rate and rotation simultaneously. In addition, since the Reynolds number can be smaller than 1, the Stokes equations are solved for this configuration using a numerical boundary integral method. The numerical results match the lubrication solution for small gaps, and determine the limits of validity for using the lubrication results.

1. Introduction

The development of micro-electro-mechanical systems (MEMS) has generated great interest in the design and demonstration of micropumps, micromotors, microactuators and other mechanical devices (Ho & Tai 1998; Wenning 1999; Aluru *et al.* 1998). Some of the applications involve fluid-structure interactions in the viscously dominated flow limit. For example, Sen, Wajerski & Gad-el-Hak (1996) proposed and demonstrated experimentally a viscous micropump that uses a rotating cylinder to generate flow between two plates. The device has been studied numerically using two-dimensional finite-element methods (Sharatchandra, Sen & Gad-el-Hak 1997) and three-dimensional finite-element software (DeCourtye, Sen & Gad-el-Hak 1998). The research reported here complements this work by using modelling and simulation methods specific to thin gaps and/or low-Reynolds-number flows, which are two limits that have potential applicability. In particular, our work addresses the lubrication limit of the viscous micropump configuration, and investigates the full Stokes flow problem since the Reynolds number of the flow based on the cylinder radius can be much less than 1. The resulting Stokes equations are solved using a boundary integral method, thus eliminating the problem of insufficient mesh generation in the gaps, that is often encountered in finite-element methods.

Consider Poiseuille flow in the space between two plates. A cylinder is introduced perpendicular to the flow and parallel to the walls. If the cylinder is not centred in

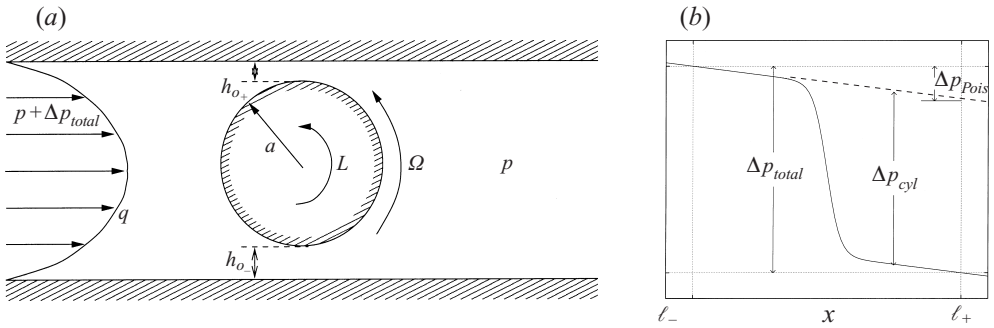

FIGURE 1. (*a*) Sketch of viscous micropump/micromotor where the flow sufficiently far upstream and downstream is parabolic. (*b*) Sketch of pressure at position x along channel, indicating the definitions of Δp_{total}, Δp_{cyl} and Δp_{Pois}; the solid line is with the cylinder and the dashed line is without the cylinder (Poiseuille flow).

the gap, it will tend to rotate due to the net tangential viscous stresses along the surface of the cylinder, as indicated in figure 1(*a*). Conversely, if the eccentrically placed cylinder is rotated by an externally applied torque, it will generate a flow in the channel and an accompanying pressure drop across the cylinder. The pressure could be measured at two locations $x = \ell_-$ upstream and $x = \ell_+$ downstream of the cylinder to determine a total pressure drop Δp_{total}. The pressure drop is denoted here as

$$p(\ell_-) - p(\ell_+) = \Delta p_{total} = \Delta p_{Pois} + \Delta p_{cyl}, \tag{1.1}$$

as shown in figure 1(*b*) where Δp_{Pois} is the pressure drop due to Poiseuille flow at the same flow rate in the absence of a cylinder, and where Δp_{cyl} is the additional pressure difference due to the cylinder. Since we can find Δp_{Pois} from the flow rate, we can characterize the entire flow using four parameters: flow rate per unit width q, rotation rate Ω, pressure drop Δp_{cyl}, and torque per unit width L applied to the cylinder. We will utilize both a force balance and a torque balance so that given two parameters we can solve for the other two. Hereinafter, our concern about pressure drop will be with that across the cylinder only, so Δp_{cyl} will be denoted simply Δp.

For example, a configuration that represents a motor is where Δp and the torque L of the load on the cylinder are given, and the rotation rate and flow rate through the device are determined. Note that in this case a pump and motor are the same device, but with different input and output parameters.

We consider the low-Reynolds-number flow limit. Since the Stokes equations are linear, there must be a linear relationship between the four parameters q, Ω, Δp, and L. We may thus construct a matrix of coefficients,

$$\mu \begin{bmatrix} A_{\Delta pq} & A_{Lq} \\ A_{\Delta p\Omega} & A_{L\Omega} \end{bmatrix} \begin{pmatrix} \Delta p \\ L \end{pmatrix} = \begin{pmatrix} q \\ \Omega \end{pmatrix}, \tag{1.2}$$

where the A are functions of geometry and allow complete characterization of the system's response. This matrix is one of six possible matrices since we are given two of the four parameters. The matrix elements can be determined analytically using a lubrication analysis, and can be calculated numerically using the boundary integral method. In § 2 we give a simple proof that $A_{\Delta p\Omega} = A_{Lq}$.

In this paper we first provide an analytical solution for this configuration using the lubrication approximation (§ 3). The full solution to the Stokes flow problem is found numerically using the boundary integral technique (§ 4), and allows the calculation

of the flow parameters with non-lubrication gap sizes. Results are summarized in § 5 where optimization of a given parameter is performed using the lubrication solution given two other parameters. The numerical solution also determines the region of validity of the lubrication approximation.

2. Reciprocal theorem

The reciprocal theorem for the Stokes equations $\nabla \cdot \boldsymbol{\sigma} = \mathbf{0}$, where $\boldsymbol{\sigma}$ is the stress tensor, states that two flows $(\boldsymbol{u}, \boldsymbol{\sigma})$ and $(\boldsymbol{u}^*, \boldsymbol{\sigma}^*)$ satisfy (see for example Kim & Karrila 1991)

$$\int_S \boldsymbol{n} \cdot \boldsymbol{\sigma} \cdot \boldsymbol{u}^* \, \mathrm{d}S = \int_S \boldsymbol{n} \cdot \boldsymbol{\sigma}^* \cdot \boldsymbol{u} \, \mathrm{d}S. \tag{2.1}$$

For the geometry shown in figure 1, the surface S is made up of three parts: the cylinder S_C, the top and bottom walls $S_\pm$, and the flat sections $S_{\ell_\pm}$ far enough upstream and downstream that the velocity profile is parabolic. On S_{ℓ_-}, $\boldsymbol{u} = u(y)\boldsymbol{e}_x$ and $\boldsymbol{n} = -\boldsymbol{e}_x$ so

$$\int_{S_{\ell_-}} \boldsymbol{n} \cdot \boldsymbol{\sigma} \cdot \boldsymbol{u}^* \, \mathrm{d}S = (p + \Delta p_{total}) \int_0^h u^*(y) \, \mathrm{d}y = (p + \Delta p_{total}) q^*, \tag{2.2}$$

and similarly

$$\int_{S_{\ell_+}} \boldsymbol{n} \cdot \boldsymbol{\sigma} \cdot \boldsymbol{u}^* \, \mathrm{d}S = -p q^*. \tag{2.3}$$

Integrals vanish on the walls where $\boldsymbol{u} = \mathbf{0}$, and on S_C, $\boldsymbol{u} = \boldsymbol{\Omega} \wedge \boldsymbol{r}$, so

$$\int_{S_C} \boldsymbol{n} \cdot \boldsymbol{\sigma} \cdot \boldsymbol{\Omega}^* \wedge \boldsymbol{r} \, \mathrm{d}S = \int_{S_C} \boldsymbol{r} \wedge (\boldsymbol{n} \cdot \boldsymbol{\sigma}) \, \mathrm{d}S \cdot \boldsymbol{\Omega}^* = L\Omega^*, \tag{2.4}$$

where $L\boldsymbol{e}_z$ is the torque per unit length applied to the cylinder and $\boldsymbol{e}_z$ is along the axis of the cylinder, directed out the page. Next write $\Delta p_{total} = \Delta p_{Pois} + \Delta p_{cyl}$, with $\Delta p_{Pois} = cq$, where c is a function of ℓ and channel height. Repeating the above steps for the right-hand side of equation (2.1) leads to (the cqq^* term cancels)

$$L\Omega^* + \Delta p_{cyl} q^* = L^* \Omega + \Delta p^*_{cyl} q. \tag{2.5}$$

Denoting Δp_{cyl} as Δp, we use equation (1.2) to eliminate q and Ω in terms of Δp and L and find

$$(L\Delta p^* - L^* \Delta p)(A_{\Delta p \Omega} - A_{Lq}) = 0. \tag{2.6}$$

Since this must hold for all possible flows, we conclude that $A_{\Delta p \Omega} = A_{Lq}$. We therefore only need to find three elements of the matrix in equation (1.2).

3. Lubrication analysis

Consider the geometry shown in figure 1, where the two gaps $h_+(x)$ and $h_-(x)$ are small compared to a, the radius of the cylinder. The velocity field is $\boldsymbol{u} = (u, v)$ and x is the direction along the channel. The steady lubrication equations for the flow in the thin gaps are

$$\mu \frac{\partial^2 u}{\partial y^2} - \frac{\partial p}{\partial x} = 0, \qquad \frac{\partial p}{\partial y} = 0, \tag{3.1a}$$

$$\frac{\partial u}{\partial x} + \frac{\partial v}{\partial y} = 0. \tag{3.1b}$$

The boundary conditions are that on the walls $\boldsymbol{u} = \boldsymbol{0}$, and on the cylinder $\boldsymbol{u} = \boldsymbol{\Omega} \wedge \boldsymbol{r}$. The solution of these equations for a non-rotating cylinder is standard (see for example Leal 1993; Keller 1964) and here we extend the calculation to account for rotation and applied torques. From equation (3.1*a*), $p = p(x)$ only. The flow velocity in the top gap is found by integrating (3.1) twice and using the boundary conditions $u_+(0) = 0$ and $u_+(h_+) = -\Omega a$. Measuring y from the wall to the cylinder, which in the top gap is directed downwards, we find

$$u_+ = \frac{1}{2\mu}\frac{\mathrm{d}p_+}{\mathrm{d}x}(y^2 - h_+ y) - \frac{\Omega a y}{h_+}. \tag{3.2}$$

The flow rate per unit width of channel is the same at every position x, and is found by integrating vertically across the gap using $q = \int_0^h u \,\mathrm{d}y$, which for the top gap is

$$q_+ = -\frac{h_+^3}{12\mu}\frac{\mathrm{d}p_+}{\mathrm{d}x} - \frac{\Omega a h_+}{2}. \tag{3.3}$$

Since q_+ is constant, the total pressure drop Δp_+ is found by integrating $\mathrm{d}p_+/\mathrm{d}x$ along the gap from $-\infty$ to $+\infty$, so

$$\Delta p_+ = -12 q_+ \mu \int_{-\infty}^{\infty} \frac{\mathrm{d}x}{h_+^3(x)} - 6\mu\Omega a \int_{-\infty}^{\infty} \frac{\mathrm{d}x}{h_+^2(x)}, \tag{3.4}$$

where $\Delta p_+ = p_{+\infty} - p_{-\infty}$. This use of integrating to $\pm\infty$ is permissible since all variations in the gap occur on the scale $(h_\pm a)^{1/2} \ll a$. With the approximation that the gap thickness varies quadratically as

$$h_+(x) \approx h_{o_+} + \frac{x^2}{2a} = h_{o_+}\left(1 + \frac{x^2}{2a h_{o_+}}\right), \tag{3.5}$$

where h_{o_+} is the minimum gap thickness, we find

$$\Delta p_+ = -\frac{9\sqrt{2}\pi\mu a^{1/2}}{2h_{o_+}^{5/2}} q_+ - \frac{3\sqrt{2}\pi\mu a^{3/2}}{h_{o_+}^{3/2}}\Omega. \tag{3.6}$$

Similarly, for the bottom gap

$$\Delta p_- = -\frac{9\sqrt{2}\pi\mu a^{1/2}}{2h_{o_-}^{5/2}} q_- + \frac{3\sqrt{2}\pi\mu a^{3/2}}{h_{o_-}^{3/2}}\Omega. \tag{3.7}$$

To close the above system of equations, we note that the total pressure drop across each gap must be equal since the variations that occur within the gap are much larger than those that occur on the scale of a outside the gap. The additional contributions to the pressure drop across the cylinder that derive from fluid motion outside the narrow gap are expected to be $O(\mu q_{max}/a^2)$, where $q_{max} = \max(q_+, q_-)$, which is small compared to the corresponding terms in equations (3.6) and (3.7). Writing $\Delta p_+ = \Delta p_- = -\Delta p$, where $\Delta p > 0$, we now have two equations with three unknowns: q_+, q_- and Ω. The torque (per unit width) is found by integrating the shear stress τ_{xy} over the surface of the cylinder, where $\tau_{xy} = \mu\partial u/\partial y\,|_{h_+}$, multiplied by the moment arm a,

$$L_+ = a\int_{-\infty}^{\infty} \tau_{xy}|_{h_+}\,\mathrm{d}x = a\int_{-\infty}^{\infty}\left(\frac{1}{2}\frac{\mathrm{d}p_+}{\mathrm{d}x}h_+ - \frac{\mu\Omega a}{h_+}\right)\mathrm{d}x. \tag{3.8}$$

Using equation (3.3) for $\mathrm{d}p_+/\mathrm{d}x$ and the parabolic profile of the gap for $h_+(x)$, we

Given	u_c
L	$L/\mu a$
Ω	Ωa
Δp	$\Delta p a/\mu$
q	q/a

TABLE 1. Characteristic velocity based on different parameters.

integrate to obtain

$$L_+ = -\frac{4\sqrt{2}\pi\mu a^{3/2}}{h_{o_+}^{1/2}}\left(\frac{3}{4}\frac{q_+}{h_{o_+}} + \Omega a\right). \tag{3.9}$$

Similarly, for the bottom gap

$$L_- = -\frac{4\sqrt{2}\pi\mu a^{3/2}}{h_{o_-}^{1/2}}\left(\frac{3}{4}\frac{q_-}{h_{o_-}} - \Omega a\right). \tag{3.10}$$

If the applied torque is L, then for steady-state operation $L + L_+ + L_- = 0$ which yields

$$L = \frac{4\sqrt{2}\pi\mu a^{3/2}}{h_{o_+}^{1/2}}\left(\frac{3q_+}{4h_{o_+}} + \Omega a\right) - \frac{4\sqrt{2}\pi\mu a^{3/2}}{h_{o_-}^{1/2}}\left(\frac{3q_-}{4h_{o_-}} - \Omega a\right). \tag{3.11}$$

It is convenient to non-dimensionalize all variables by using the characteristic length a, the shear viscosity μ, and a characteristic velocity u_c, and to denote the dimensionless variables using a superscript $*$:

$$\left.\begin{aligned} &\Delta p = \Delta p^* \frac{\mu u_c}{a}, \qquad \Omega = \frac{u_c}{a}\Omega^*, \quad L = \mu u_c a L^*, \\ &q_\pm = u_c a q_\pm^*, \qquad h_{0_\pm} = a h_{0_\pm}^*. \end{aligned}\right\} \tag{3.12}$$

The characteristic velocity is determined by one of the given four flow parameters and is listed in table 1. Also, it is useful to introduce two geometric parameters

$$\delta = h_{o_+}^* + h_{o_-}^*, \quad \eta = \frac{h_{o_+}^*}{\delta}, \tag{3.13}$$

from which $h_{o_-}^*/\delta = 1 - \eta$ follows. The lubrication approximation requires that $\delta \ll 1$ and shortly the scaling involving δ will be shown. Notice that η measures the eccentricity, so varies from 0 to 1. Finally, the three equations for dimensionless q_+^*, q_-^* and Ω^* in terms of Δp^*, L^* and the geometrical factors η and δ are

$$\frac{3q_+^*}{2\eta} + \Omega^*\delta = \frac{\Delta p^* \eta^{3/2}\delta^{5/2}}{3\sqrt{2}\pi}, \tag{3.14a}$$

$$\frac{3q_-^*}{2(1-\eta)} - \Omega^*\delta = \frac{\Delta p^* (1-\eta)^{3/2}\delta^{5/2}}{3\sqrt{2}\pi}, \tag{3.14b}$$

$$\frac{3q_+^*}{\eta^{3/2}} - \frac{3q_-^*}{(1-\eta)^{3/2}} + \frac{4\left((1-\eta)^{1/2} + \eta^{1/2}\right)\Omega^*\delta}{\eta^{1/2}(1-\eta)^{1/2}} = \frac{L^*\delta^{3/2}}{\sqrt{2}\pi}. \tag{3.14c}$$

Equation (3.14) provides a complete lubrication characterization of the micropump

device. Dropping the * and solving for Ω, q_+ and q_- yields

$$q_+ = \frac{2\Delta p\delta^{5/2}}{9\sqrt{2}\pi}\frac{\eta^{3/2}\left(\eta^{3/2}+(1-\eta)^{1/2}(3\eta-1)\right)}{\eta^{1/2}+(1-\eta)^{1/2}} - \frac{L\delta^{3/2}}{3\sqrt{2}\pi}\frac{\eta^{3/2}(1-\eta)^{1/2}}{\eta^{1/2}+(1-\eta)^{1/2}}, \tag{3.15a}$$

$$q_- = \frac{2\Delta p\delta^{5/2}}{9\sqrt{2}\pi}\frac{(1-\eta)^{3/2}\left((1-\eta)^{3/2}+\eta^{1/2}(2-3\eta)\right)}{\eta^{1/2}+(1-\eta)^{1/2}} + \frac{L\delta^{3/2}}{3\sqrt{2}\pi}\frac{\eta^{1/2}(1-\eta)^{3/2}}{\eta^{1/2}+(1-\eta)^{1/2}}, \tag{3.15b}$$

$$\Omega = \frac{\Delta p\delta^{3/2}}{3\sqrt{2}\pi}\left((1-\eta)\eta^{1/2}-\eta(1-\eta)^{1/2}\right) + \frac{L\delta^{1/2}}{2\sqrt{2}\pi}\frac{\left((1-\eta)\eta^{1/2}-\eta(1-\eta)^{1/2}\right)}{1-2\eta}. \tag{3.15c}$$

It may be observed that $q_+(\eta,\delta;\Delta p,L) = q_-(1-\eta,\delta;\Delta p,-L)$ as expected from symmetry. The total flow rate $q = q_+ + q_-$, so we will refer to q from now on. The above equations lead to

$$q = \frac{2\Delta p\delta^{5/2}}{9\sqrt{2}\pi}\left(\eta^{1/2}+(1-\eta)^{1/2}\right)\left(3\eta^2-3\eta+1\right) + \frac{L\delta^{3/2}}{3\sqrt{2}\pi}\left(\frac{(1-2\eta)\eta^{1/2}(1-\eta)^{1/2}}{\eta^{1/2}+(1-\eta)^{1/2}}\right), \tag{3.16a}$$

$$\Omega\delta = \frac{\Delta p\delta^{5/2}}{3\sqrt{2}\pi}\left(\frac{(1-2\eta)\eta^{1/2}(1-\eta)^{1/2}}{\eta^{1/2}+(1-\eta)^{1/2}}\right) + \frac{L\delta^{3/2}}{2\sqrt{2}\pi}\left(\frac{\eta^{1/2}(1-\eta)^{1/2}}{\eta^{1/2}+(1-\eta)^{1/2}}\right), \tag{3.16b}$$

which corresponds to the matrix representation in equation (1.2). From the reciprocity of Stokes flow (§ 2), $A_{\Delta p\Omega} = A_{Lq}$, so there are only three coefficients that characterize the geometry. One can see that the matrix elements are symmetric about $\eta = 1/2$.

In fact, equation (1.2) is one of the six possible matrix representations of the relationships among the four parameters. For example, one could perform Gauss–Jordan elimination to find a pair of equations involving $(q,\Delta p,\Omega)$ and $(L,\Delta p,\Omega)$. There are only four relations involving three of the four parameters, and these are listed below for the reader's convenience. To simplify the relations, we have substituted the factors involving δ with

$$\Delta\hat{p} = \frac{\Delta p\delta^{5/2}}{\pi\sqrt{2}}, \quad \hat{L} = \frac{L\delta^{3/2}}{\pi\sqrt{2}}, \quad \hat{\Omega} = \Omega\delta, \tag{3.17}$$

and $\hat{q} = q$ for consistency. Note that a given system has two equations and two unknowns, so it is left to the reader to choose the pair of relations for their particular device. The four relations are

$$(\eta^{5/2}+(1-\eta)^{5/2})\hat{L} - \frac{2(\eta^{1/2}+(1-\eta)^{1/2})^2(3\eta^2-3\eta+1)}{\eta^{1/2}(1-\eta)^{1/2}}\hat{\Omega} + 3(1-2\eta)\hat{q} = 0, \tag{3.18a}$$

$$3\hat{L} - \frac{6(\eta^{1/2}+(1-\eta)^{1/2})\hat{\Omega}}{\eta^{1/2}(1-\eta)^{1/2}} + 2(1-2\eta)\Delta\hat{p} = 0, \tag{3.18b}$$

$$9\hat{q} - 2(\eta^{5/2}+(1-\eta)^{5/2})\Delta\hat{p} - 6(1-2\eta)\hat{\Omega} = 0, \tag{3.18c}$$

$$9\hat{q} - 2(\eta^{1/2}+(1-\eta)^{1/2})(3\eta^2-3\eta+1)\Delta\hat{p} - \frac{3(1-2\eta)\eta^{1/2}(1-\eta)^{1/2}}{(\eta^{1/2}+(1-\eta)^{1/2})}\hat{L} = 0. \tag{3.18d}$$

There is a special case when the cylinder is centred ($\eta = 1/2$) for which the right-most terms vanish and the equations decouple. The result is $\hat{L} = 4\sqrt{2}\hat{\Omega}$ and $\Delta\hat{p} = 9\sqrt{2}\hat{q}$,

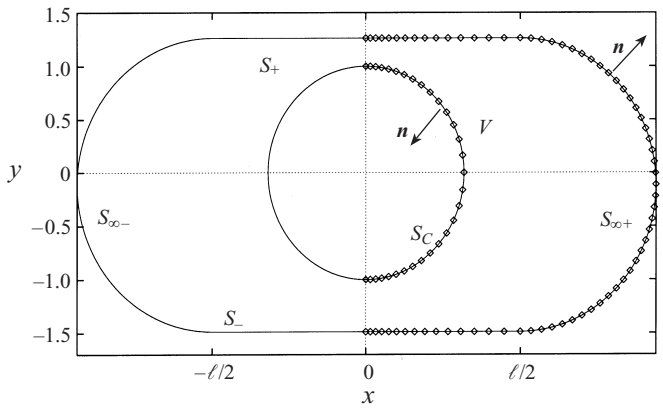

FIGURE 2. Boundary used for the integral equation solution: the solid line is the full contour of integration, and points show the half-contour used in the numerics when exploiting symmetry.

so $\Delta\hat{p}$ is not independent of $\hat{q}$, and $\hat{L}$ is not independent of $\hat{\Omega}$. At the end of §4 we compare the above analytical results and our own Stokes flow calculations with published finite-Reynolds-number finite-element numerical simulations. We will see that even for $O(1)$ Reynolds numbers there is good agreement for $\delta < 0.2$.

4. Solution using a boundary integral method

In this section, the full Stokes flow problem with arbitrary gap sizes is solved numerically. The fluid in the device is enclosed by a boundary S shown in figure 2. In this case, the boundary S consists of two walls S_+ and S_- of length ℓ, two semicircular arcs $S_{\infty+}$ and $S_{\infty-}$ at $x = \pm\ell/2$, and a circular cylinder S_C centred at the origin. Over $S_{\infty+}$ and $S_{\infty-}$, the fluid velocity is defined to be parabolic flow, denoted $\boldsymbol{U}_P$. The length ℓ is chosen to be large enough that the pressure gradient at $x = \ell/2$ is very nearly constant. The solution is found using the boundary integral equation for Stokes flow in a volume of fluid V bounded by S,

$$\int_S \boldsymbol{n}\cdot\boldsymbol{\sigma}\cdot\boldsymbol{J}\,\mathrm{d}S - \int_S \boldsymbol{n}\cdot\boldsymbol{K}\cdot\boldsymbol{u}\,\mathrm{d}S = \begin{cases} \boldsymbol{u}(\boldsymbol{x}_0), & \boldsymbol{x}_0 \in V \\ \frac{1}{2}\boldsymbol{u}(\boldsymbol{x}_0), & \boldsymbol{x}_0 \in S \\ \boldsymbol{0}, & \boldsymbol{x}_0 \notin V, \end{cases} \tag{4.1}$$

where $\boldsymbol{n}$ is the unit normal pointing out of the fluid (see Youngren & Acrivos 1975; Pozrikidis 1992; Tanzosh, Manga & Stone 1992). All variables are made dimensionless using a and u_c (see table 1). For two-dimensional flows, the tensors $\boldsymbol{J}$ and $\boldsymbol{K}$ are

$$\boldsymbol{J} = \frac{1}{4\pi}\left(\boldsymbol{I}\log r - \frac{\boldsymbol{rr}}{r^2}\right), \quad \boldsymbol{K} = \frac{1}{\pi}\frac{\boldsymbol{rrr}}{r^4}, \tag{4.2}$$

which are the fundamental solutions to Stokes flow due to a point force acting at $\boldsymbol{x}_0$, where $\boldsymbol{r} = \boldsymbol{x} - \boldsymbol{x}_0$ and $r = |\boldsymbol{r}|$. Since $\boldsymbol{u} = \boldsymbol{0}$ on the walls and $\boldsymbol{u} = \boldsymbol{\Omega}\wedge\boldsymbol{r}$ on the cylinder, the boundary integral equation reduces to

$$\int_S \boldsymbol{f}\cdot\boldsymbol{J}\,\mathrm{d}S - \int_{S_{\infty\pm}} \boldsymbol{n}\cdot\boldsymbol{K}\cdot\boldsymbol{u}\,\mathrm{d}S = \begin{cases} \boldsymbol{\Omega}\wedge\boldsymbol{r}, & \boldsymbol{x}_0 \in S_C \\ \frac{1}{2}\boldsymbol{U}_P(\boldsymbol{x}_0), & \boldsymbol{x}_0 \in S_{\infty\pm} \\ \boldsymbol{0}, & \boldsymbol{x}_0 \in S_\pm, \end{cases} \tag{4.3}$$

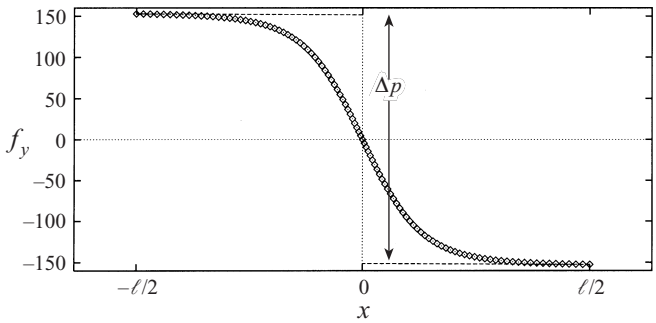

FIGURE 3. Vertical component of $\boldsymbol{f}$ along the wall, equal to the pressure in the fluid, used to calculate Δp, the pressure drop in excess of the losses due to Poiseuille flow over a length ℓ. This simulation had $L = 0$.

where $\boldsymbol{f} = \boldsymbol{n} \cdot \boldsymbol{\sigma}$, represents the unknown traction per unit width acting on the boundary.

To solve equation (4.3) for $\boldsymbol{f}$, the boundary is discretized into n nodes, as shown on the right-hand side of figure 2, which are described using an arclength-like parameter s that increases clockwise along the outer and inner boundaries. The unknown force $\boldsymbol{f}$ is approximated linearly by

$$\boldsymbol{f}(s) = \sum_{k=1}^{n} w_k(s) f_{xk} \boldsymbol{e}_x + \sum_{k=1}^{n} w_k(s) f_{yk} \boldsymbol{e}_y, \tag{4.4}$$

where the weight function w_k is defined by

$$w_k(s) = \begin{cases} 1 - |s - k| & k - 1 \leqslant s \leqslant k + 1 \\ 0 & (s < k - 1) \cup (k + 1 < s). \end{cases} \tag{4.5}$$

The boundary is described using lines and circular arcs. The nodal spacing is chosen to vary quadratically along S_C and $S_{\pm}$, so that the node density in the gap is high enough to resolve the lubrication flow. Finding a way to resolve the flow in the thin gaps enabled this work to study $O(1)$ gaps as well as the narrow lubrication regime. In the lubrication limit, the lowest resolution was required for $\delta\eta = 1$, for which $n \approx 440$, and the highest resolution was for $\delta\eta = 0.015$ for which $n \approx 1700$. A set of $2n$ linear equations is generated by taking $\boldsymbol{x}_0$ to be each node $\boldsymbol{x}_k$ and solving both components of equation (4.3) for the unknowns f_{xk} and f_{yk} at each node. The left–right symmetry of the problem is exploited to reduce the computation time by a factor of eight, since the matrix inversion uses a number of calculations proportional to n^3.

The resulting dimensionless extra pressure drop across the cylinder Δp is

$$\Delta p = f_y(\ell/2) - f_y(-\ell/2) - \frac{12\ell}{(2 + \delta)^3}, \tag{4.6}$$

which is independent of ℓ and where the last term is the pressure drop due to Poiseuille flow in a channel of height $2 + \delta$ and length ℓ. Figure 3 shows a typical plot of f_y, which at the planar wall is equal to the pressure.

The resulting dimensionless torque per unit width $\boldsymbol{L} = L\boldsymbol{e}_z$ is found by integrating the tangential stresses over the surface of the cylinder,

$$L = \int_0^{2\pi} (f_y \cos\theta - f_x \sin\theta)\, \mathrm{d}\theta. \tag{4.7}$$

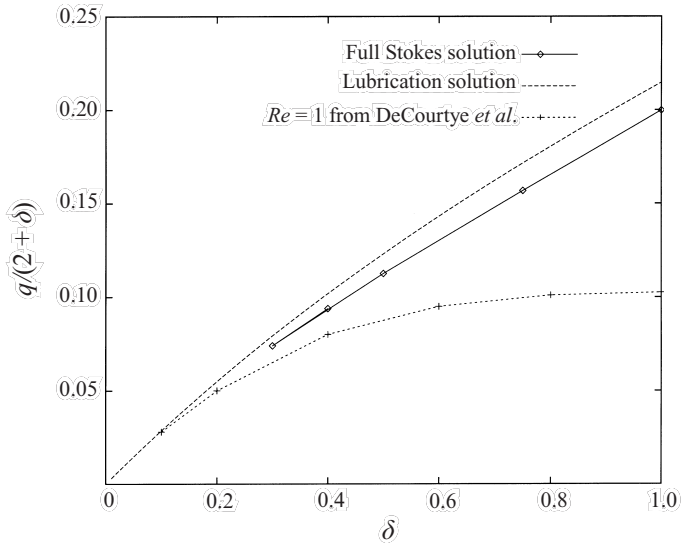

FIGURE 4. Comparison between lubrication solution, Stokes solution and $Re = 1$ solution from DeCourtye *et al.* (1998) for the bulk velocity $q/(2+\delta)$ when $\eta = 0.05$, $\Delta p = \Omega = 1$; the transverse dimension of the channel is infinite.

The code was checked using Poiseuille flow, corresponding to the case where the radius of the cylinder is zero, and circular Couette flow (Batchelor 1967) corresponding to the case where the net flow rate $q = 0$ and the length of the wall $\ell = 0$.

We close this section by providing in figure 4 a comparison with published numerical results from the literature. DeCourtye *et al.* (1998) report the average velocity for an infinitely wide channel (their figure 4), with $\eta = 0.05$, dimensionless $\Delta p = \Omega = 1$ and $Re = 2\Omega a^2/\nu = 1$. Since the average velocity is $q/(2+\delta)$, figure 4 shows that for small δ the Stokes and lubrication solutions tend to the results from DeCourtye *et al.* (1998), and that for $\delta > 0.4$, our solutions continue to increase monotonically while the $Re = 1$ solution plateaus.

5. Results

In this section, we report results for typical operating conditions using the lubrication approximation. In addition, we use the results from the lubrication analysis to calculate optimal operating flow parameters and geometry. We also determine the region of validity of the lubrication approximation by comparing it to the full numerical solution of the Stokes equations.

5.1. *Zero rotation using the lubrication solution*

A simple case of the lubrication solution is where the rotation rate is zero. Given the flow rate, equation (3.18) reduces to

$$\Delta\hat{p} = \frac{9\hat{q}}{2}\left(\frac{1}{\eta^{5/2} + (1-\eta)^{5/2}}\right), \tag{5.1a}$$

$$\hat{L} = -3\hat{q}\left(\frac{1-2\eta}{\eta^{5/2} + (1-\eta)^{5/2}}\right). \tag{5.1b}$$

Figure 5 shows these relationships plotted versus η, where the maximum and minimum are shown as squares. The extremum of $\Delta\hat{p}/\hat{q}$ occurs at $\eta = 1/2$ and the extremum

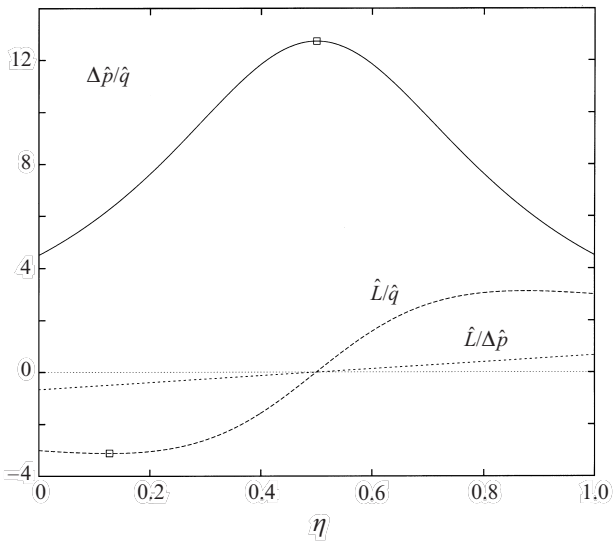

FIGURE 5. For zero rotation, the three ratios $\Delta\hat{p}/\hat{q}$, $\hat{L}/\hat{q}$ and $\hat{L}/\Delta\hat{p}$ are shown as functions of η, the geometrical factor denoting the eccentric position of the cylinder in the channel. A maximum or minimum is shown as a square on the plot.

of $\hat{L}/\hat{q}$ occurs at $(3-\sqrt{5})/6 \approx 0.1273$. There are three ways to use these results. For example, if the flow rate per unit width q is specified, then $u_c = q/a$, and $\hat{q} = 1$ so the dimensional pressure drop $\Delta p = \Delta\hat{p}\,\mu q\pi\sqrt{2}/(a^2\delta^{5/2})$ and $L = \hat{L}\,\mu q\pi\sqrt{2}/\delta^{3/2}$. Similarly, one could specify Δp or L.

5.2. *Zero torque using the lubrication solution*

Another simple case is that of zero applied torque, in which case the cylinder rotates freely due to the flow. Equation (3.18) reduces to

$$\hat{\Omega} = \frac{(1-2\eta)\eta^{1/2}(1-\eta)^{1/2}}{3(\eta^{1/2}+(1-\eta)^{1/2})}\Delta\hat{p}, \tag{5.2a}$$

$$\hat{q} = \frac{2}{9}\left(\eta^{1/2}+(1-\eta)^{1/2}\right)\left(3\eta^2-3\eta+1\right)\Delta\hat{p}. \tag{5.2b}$$

As in the previous section, there are three ways to utilize these equations, corresponding to whether q, Δp or Ω is specified. Figure 6 shows these relationships, which are symmetric about $\eta = 1/2$. The extremum and corresponding η for each curve can be determined analytically and are listed in table 2 along with the corresponding ratios h_{o_-}/h_{o_+}.

In physical terms, the maximizing of $\hat{\Omega}/\Delta\hat{p}$ when $h_{o_-}/h_{o_+} \approx 6.85$ means that the bottom gap must be about seven times the size of the top gap for the rotation rate to be maximized for a given pressure drop. This conclusion is justified by observing that the rotation goes to zero when the cylinder approaches the wall and is again zero when the cylinder is centred, so a maximum must exist in between. The second case in table 2 shows that the bottom gap must be about 60 times the top gap to obtain the maximum flow rate. This conclusion is justified by observing that as the cylinder is placed more eccentrically, more fluid is dragged through the large gap by rotation. Close to the wall though, the cylinder ceases to rotate and the extra flow from the rotation is lost, so the maximum flow rate is expected when the cylinder is a short

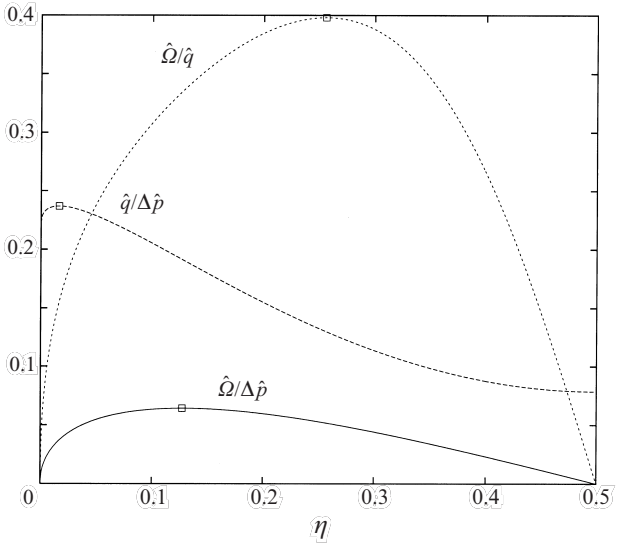

FIGURE 6. For zero torque, the three ratios $\hat{\Omega}/\Delta\hat{p}$, $\hat{q}/\Delta\hat{p}$ and $\hat{\Omega}/\hat{q}$ are shown as functions of η, the geometrical factor denoting the eccentric position of the cylinder in the channel. Maxima are shown as squares on the plot, and due to the symmetry, $\eta \leqslant 0.5$ is shown only.

Ratio	Extremum	$\eta_{extremum}$	h_{o_-}/h_{o_+}
$\hat{\Omega}/\Delta\hat{p}$	0.0642	$(3-\sqrt{5})/6 \approx 0.127$	6.85
$\hat{q}/\Delta\hat{p}$	0.237	$(15-\sqrt{93+48\sqrt{6}})/30 \approx 0.0163$	60.4
$\hat{\Omega}/\hat{q}$	0.398	0.256	2.91

TABLE 2. Ratio and η at each extremum when $\hat{L}=0$, and the corresponding ratio h_{o_-}/h_{o_+}.

distance away from the wall. Note that the critical η is different for each case, so a device cannot be developed that achieves maximum flow rate and rotation simultaneously. By examining figures 7(*a*) and 10(*c*) in the next subsection, this conclusion also holds for non-zero applied torques.

5.3. *Optimization by varying* η

The previous case was for zero torque, and the next question addressed is how the optimum parameter values listed in table 2 change for various non-zero torques. For example, the extremum of $\hat{\Omega}/\Delta\hat{p}$ now depends on the torque, $\hat{L}/\Delta\hat{p}$, from a rearrangement of equation (3.18). One can determine the η for which $\hat{\Omega}/\Delta\hat{p}$ is a maximum or minimum for a given $\hat{L}/\Delta\hat{p}$. Equation (3.18) can be rearranged to form three ratios by dividing all terms by each of three variables: $\hat{\Omega}/\Delta\hat{p} \propto \hat{L}/\Delta\hat{p}$, $\hat{\Omega}/\hat{L} \propto \Delta\hat{p}/\hat{L}$, and $\hat{L}/\hat{\Omega} \propto \Delta\hat{p}/\hat{\Omega}$. This exercise can be performed for all possibilities of the four equations in (3.18), yielding twelve plots. Figures 7–10 show all twelve plots relating the ratios of parameters $\hat{\Omega}$, $\Delta\hat{p}$, $\hat{q}$, and $\hat{L}$, and some corresponding extrema. These results provide a comprehensive summary of the micropump flow configuration, including the parameters that provide optimization. The figures can be used to learn something about the physical problem, given two parameters.

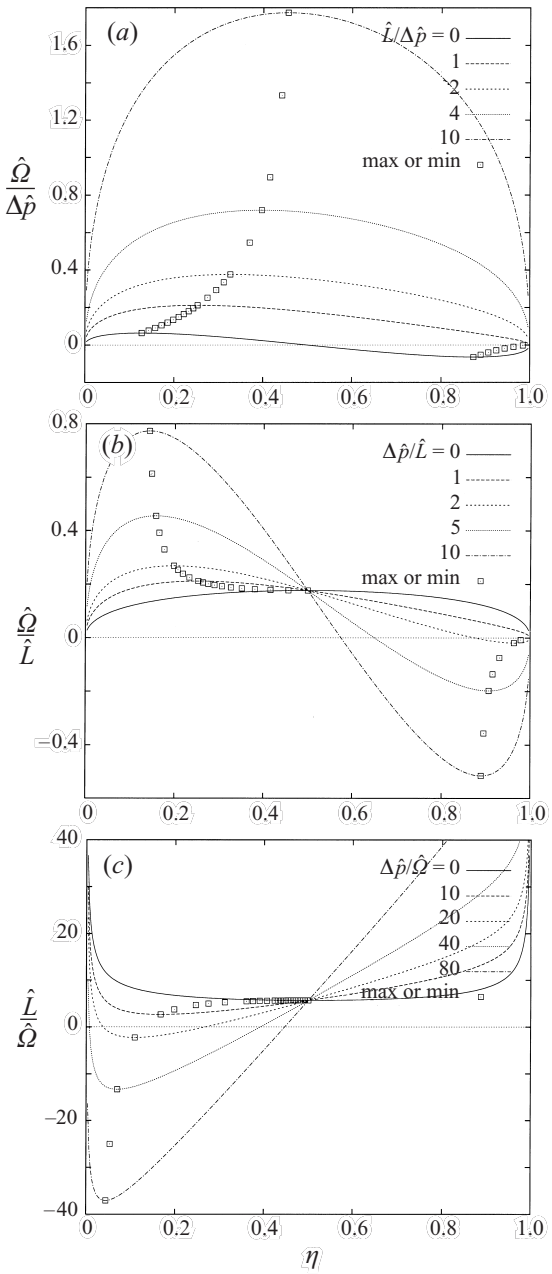

FIGURE 7. Ratios from the $\hat{\Omega} - \Delta\hat{p} - \hat{L}$ equation: (*a*) $\hat{\Omega}/\Delta\hat{p}$ versus η for various $\hat{L}/\Delta\hat{p}$, (*b*) $\hat{\Omega}/\hat{L}$ versus η for various $\Delta\hat{p}/\hat{L}$, and (*c*) $\hat{L}/\hat{\Omega}$ versus η for various $\Delta\hat{p}/\hat{\Omega}$.

For example, figure 7(*a*) shows that as the applied torque increases from zero, the location where maximum rotation is achieved moves further from the wall. Also, as the ratio $\hat{L}/\Delta\hat{p}$ becomes large, the behaviour of the ratio $\hat{\Omega}/\Delta\hat{p}$ becomes symmetrical about the centre of the channel, meaning that torque determines the rotation rather than pressure drop. Figure 8(*a*) also shows the tendency towards symmetry for large torque, but relative to the flow rate. One could choose to design a device where $\hat{L}/\hat{q}$

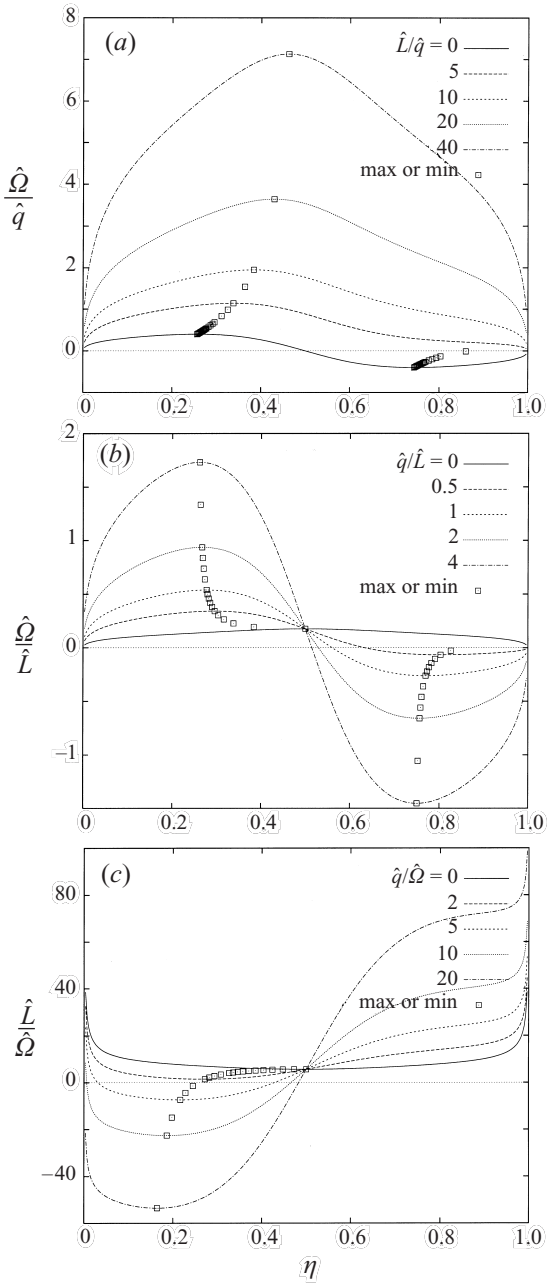

FIGURE 8. Ratios from the $\hat{q} - \hat{\Omega} - \hat{L}$ equation: (*a*) $\hat{\Omega}/\hat{q}$ versus η for various $\hat{L}/\hat{q}$, (*b*) $\hat{\Omega}/\hat{L}$ versus η for various $\hat{q}/\hat{L}$, and (*c*) $\hat{L}/\hat{\Omega}$ versus η for various $\hat{q}/\hat{\Omega}$.

is known, and then one would examine figures 8(*a*) and 10(*b*). For example, if large $\Delta\hat{p}$ is desired and $\hat{L}/\hat{q} = 20$, then $\eta \approx 0.6$ would be appropriate, and also $\hat{\Omega}/\hat{q}$ would not be too far from its maximum.

The case of zero flow rate can also be discussed here, which corresponds to the case where the flow in the top gap is equal in magnitude but opposite in direction to the flow in the bottom gap. Figures 9(*b*,*c*) and 10(*a*,*c*) illustrate several choices

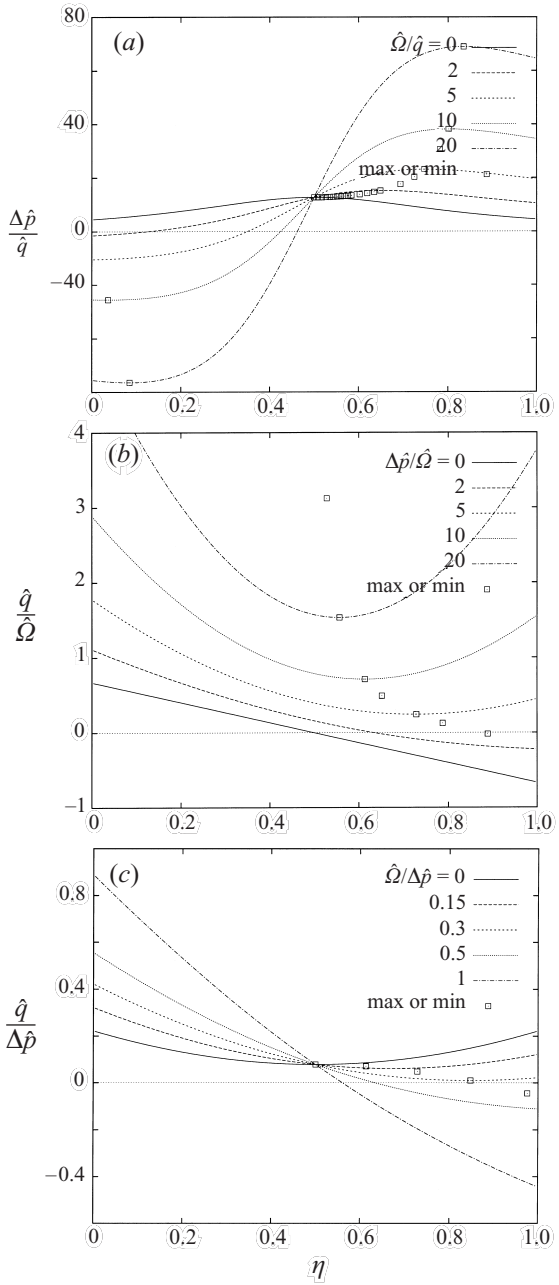

FIGURE 9. Ratios from the $\hat{q} - \Delta\hat{p} - \hat{\Omega}$ equation: (*a*) $\Delta\hat{p}/\hat{q}$ versus η for various $\hat{\Omega}/\hat{q}$, (*b*) $\hat{q}/\hat{\Omega}$ versus η for various $\Delta\hat{p}/\hat{\Omega}$, and (*c*) $\hat{q}/\Delta\hat{p}$ versus η for various $\hat{\Omega}/\Delta\hat{p}$.

for other parameters that permit zero net flow, and certain ranges of parameters for which zero flow is not possible. For example, for $\hat{L}/\Delta\hat{p} \geqslant 2.5$, zero flow is possible when $\eta \approx 0.75$, and for larger values of $\hat{L}/\Delta\hat{p}$ there are two choices of η which result in zero flow. In fact, the lower of the two η values would be the one a designer would choose in order to get a greater rotation rate, as shown by figure 7(*a*).

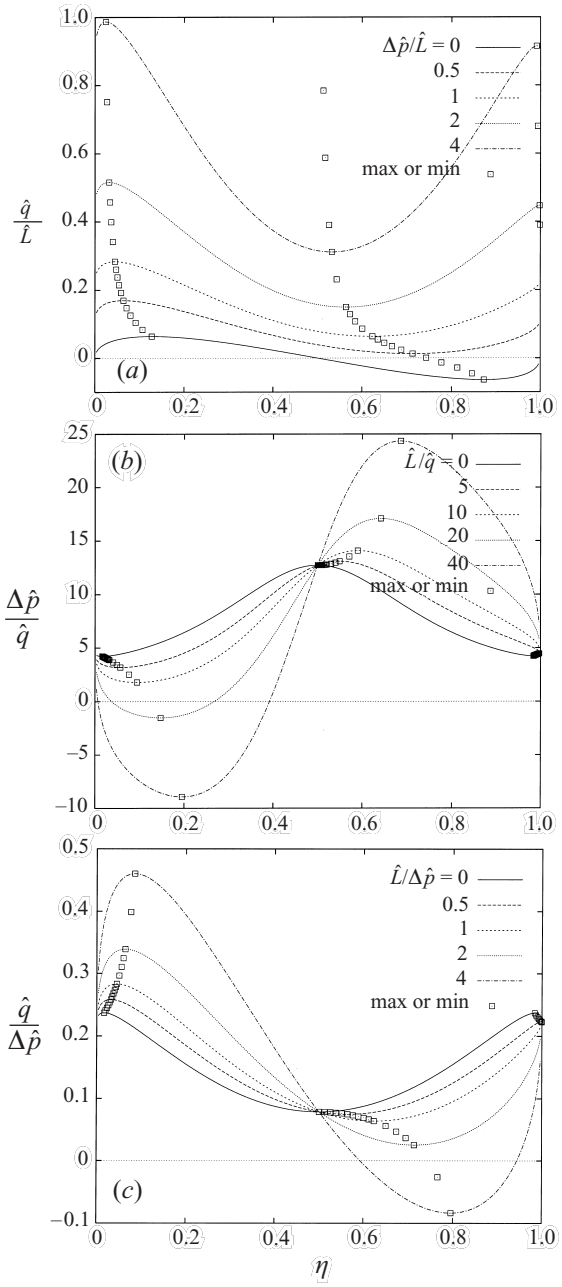

FIGURE 10. Ratios from the $\hat{q} - \Delta\hat{p} - \hat{L}$ equation: (*a*) $\hat{q}/\hat{L}$ versus η for various $\Delta\hat{p}/\hat{L}$, (*b*) $\Delta\hat{p}/\hat{q}$ versus η for various $\hat{L}/\hat{q}$, and (*c*) $\hat{q}/\Delta\hat{p}$ versus η for various $\hat{L}/\Delta\hat{p}$.

5.4. *Optimization by varying* δ

The second of the two geometrical parameters is δ, denoting the ratio of the sum of the gaps to the radius of the cylinder (equation (3.13)). By varying δ while keeping the eccentricity η constant, local maxima or minima of the flow parameters can be found. Using both optimizations, an extremum of a flow parameter such as rotation

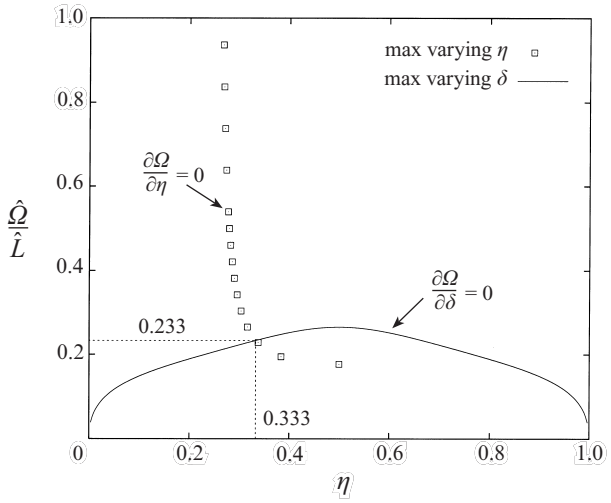

FIGURE 11. The intersection of two plots determines that $\partial\Omega/\partial\eta = 0$ and $\partial\Omega/\partial\delta = 0$ at $\eta = 0.333$ and $\hat{\Omega}/\hat{L} = 0.233$.

rate can be found in all of (η, δ)-space where $\partial\Omega/\partial\eta = 0$ and $\partial\Omega/\partial\delta = 0$, holding all other parameters fixed. For example, with q and L constant, $\Omega = f(\eta, \delta)$ only. In this section, we will demonstrate this case to illustrate the idea, and leave it to the reader to determine other optimizations as required.

Equation (3.18) can be written as

$$A\Omega\delta = Bq + CL\delta^{3/2}, \tag{5.3}$$

where A, B, and C are functions of η. An extremum of Ω occurs when

$$A\frac{\partial\Omega}{\partial\delta} = -Bq\delta^{-2} + \tfrac{1}{2}CL\delta^{-1/2} = 0, \tag{5.4}$$

so $\hat{q}/\hat{L} = C\pi/B\sqrt{2}$. The extremum is therefore

$$\frac{\hat{\Omega}}{\hat{L}} = \frac{3\pi\sqrt{2}C}{2A} = \frac{3\left(\eta^{5/2} + (1-\eta)^{5/2}\right)\eta^{1/2}(1-\eta)^{1/2}}{4\left(\eta^{1/2} + (1-\eta)^{1/2}\right)^2\left(3\eta^2 - 3\eta + 1\right)}. \tag{5.5}$$

In the previous subsection, figure 8(b) showed extrema of $\hat{\Omega}/\hat{L}$ versus η for various $\hat{q}/\hat{L}$. Plotting these extrema and equation (5.5) in figure 11, we conclude that the maximum of Ω in (η, δ)-space occurs at the intersection where $\eta = 0.333$ and $\hat{\Omega}/\hat{L} = 0.233$. The value of δ is then determined using the given L and the desired Ω. These values for the optimal η and δ are a result of the lubrication approximation and so require $\delta \ll 1$ (see § 5.6). The exact optimal geometry can be found using the full two-dimensional Stokes problem shown in § 4 which can be solved iteratively in the neighbourhood of the optimum determined by the lubrication approximation.

5.5. *Zero rotation using the boundary integral solution*

Considering the case $\Omega = 0$, we compare numerical results with predictions from lubrication theory, equation (5.1). The two input variables into the boundary integral simulation are the flow rate q and the rotation rate of the cylinder Ω and we choose

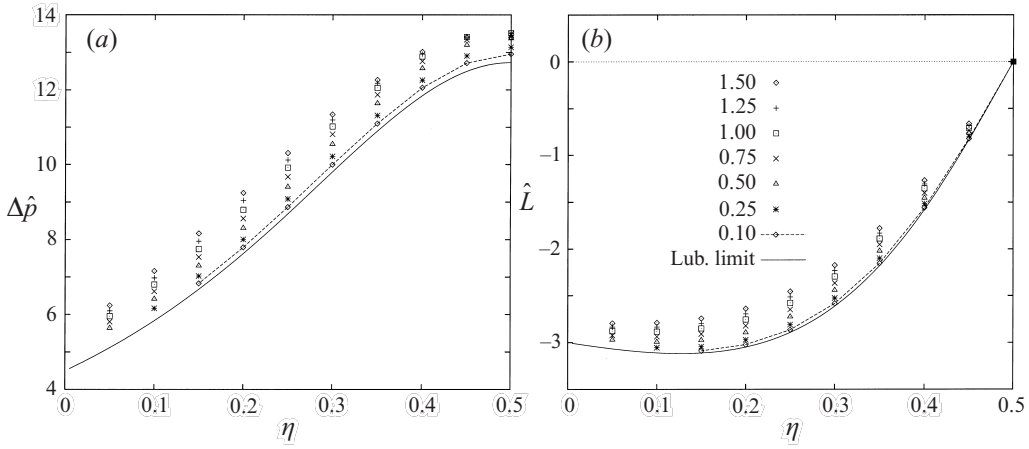

FIGURE 12. (*a*) Pressure drop and (*b*) torque from the boundary integral simulations where the rotation rate is zero, for various δ at several η. As δ becomes small, $\Delta\hat{p}$ and $\hat{L}$ approach the lubrication limit.

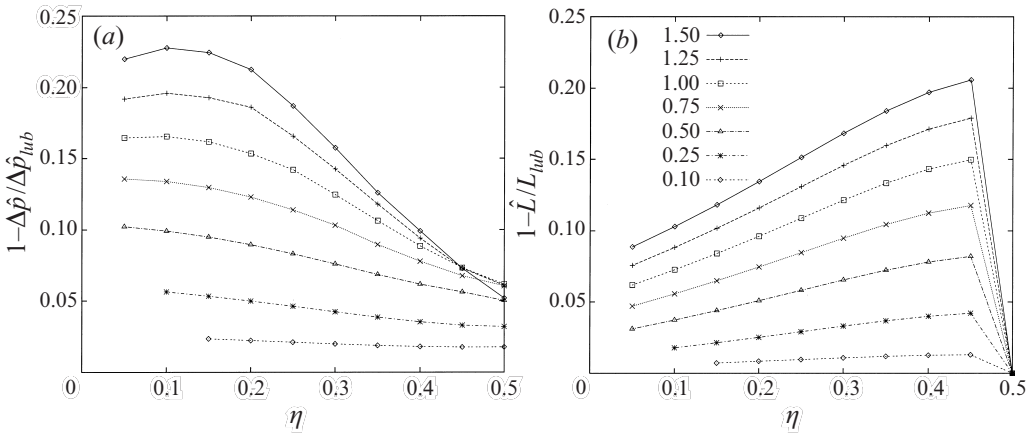

FIGURE 13. Relative error of (*a*) pressure drop and (*b*) torque between the results from the boundary integral simulations and the lubrication analysis.

the characteristic velocity $u_c = q/a$, so $\hat{q} = 1$. Figure 12(*a,b*) shows that the numerical solution indeed approaches the lubrication limit as δ becomes small. The solutions are symmetric about $\eta = 1/2$. Figure 13(a, b) shows the relative error between the results from the boundary integral simulations and the lubrication results. These results show that the relative error in pressure drop is at most 10% for $\delta = 0.5$, corresponding to the geometry where the sum of the gaps is half the radius of the cylinder. Even for $\delta = 1.5$, the largest error is less than 23%, and the error when centred ($\eta = 1/2$) is below 7%. The error in the torque is similarly bounded to about 10% when $\delta = 0.5$. This result suggests that the expression for the pressure drop using the simple analytical result from lubrication theory is a good approximation to the full solution for $\delta \leqslant O(1)$, and improves as δ becomes small, as one expects in thin geometries.

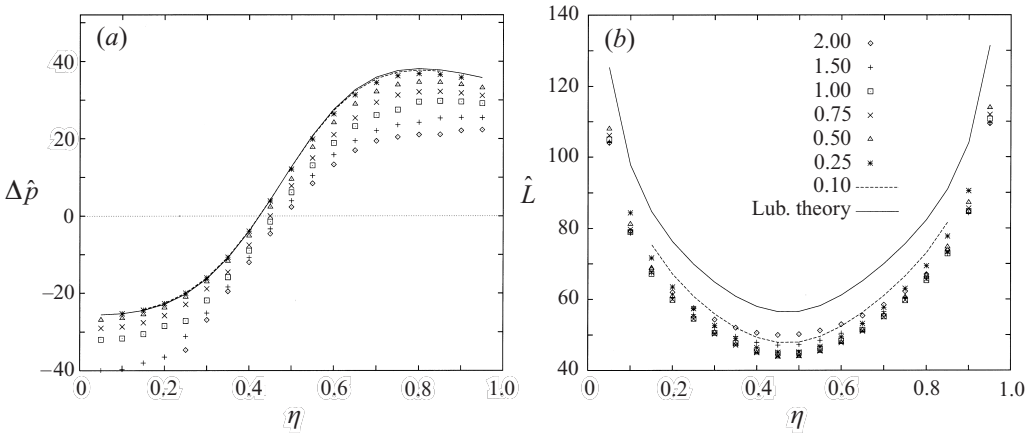

FIGURE 14. (*a*) Pressure drop and (*b*) torque from boundary integral simulations where $\hat{\Omega} = 10$ for various δ at several η. As δ becomes small, $\Delta\hat{p}$ and $\hat{L}$ approach the lubrication limit, although $\hat{L}$ approaches more slowly than $\Delta\hat{p}$.

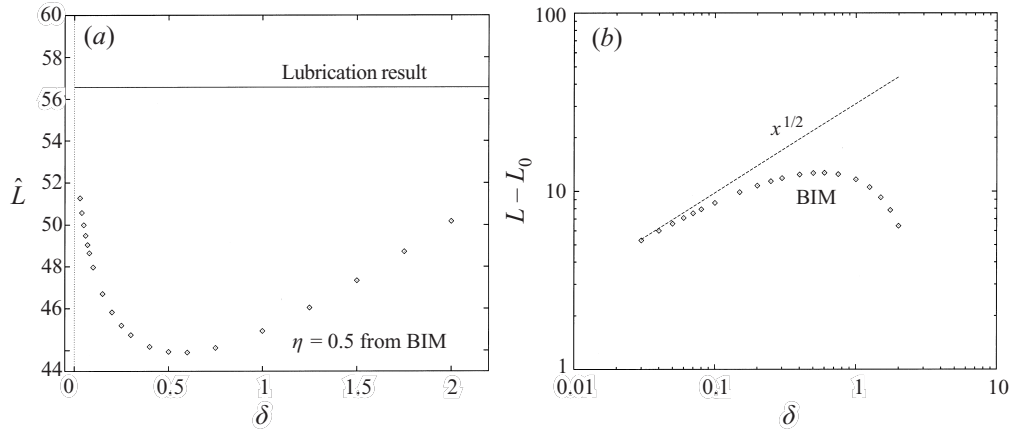

FIGURE 15. (*a*) Torque at $\eta = 1/2$ for $\hat{\Omega} = 10$ and $q = 1$. Comparison between the result using boundary integrals and lubrication analysis. (*b*) Log–log plot to show the exponent of δ in the second-order correction term for the torque is $1/2$ for small δ.

5.6. *Non-zero rotation and non-zero torque*

To compare geometries with various δ when the rotation rate is non-zero, the product $\Omega\delta = \hat{\Omega}$ must be constant. Figure 14(*a*,*b*) shows the boundary integral results for $\hat{\Omega} = 10$, $\hat{q} = 1$, and $0.1 \leqslant \delta \leqslant 2.0$ compared to the lubrication limit. When the cylinder rotates, although the pressure drop prediction is accurate, the torque result shows a noticeable difference and a slower approach to the lubrication prediction.

Closer examination of the data in figure 14(*b*) is required to observe the trend towards the lubrication limit for the torque. Focusing on the $\eta = 1/2$ geometry, several boundary integral simulations were performed at various δ to determine the torque. Values of $\delta < 0.05$ require a significant number of nodes in the gap for adequate resolution, so such geometries take increasingly more time to calculate accurately. Figure 15(*a*) shows the trend of the boundary integral result compared to

the lubrication limit. The lubrication result is given by $\hat{L} = 4\sqrt{2}\hat{\Omega}$ from equation (3.18) with $\eta = 1/2$. For $\hat{\Omega} = 10$, $\hat{L} = 40\sqrt{2} = 56.569$. The greatest difference is about 22%, when $\delta \approx 0.5$. For smaller δ, the boundary integral result tends toward the lubrication limit.

A reason for the disagreement is that the lubrication approximation neglects the flow in the far field, which is outside the region of the gap and is generated by viscous shear stresses from the rotation of the cylinder. Consider a second-order correction term to the torque, in an expansion in some power of δ,

$$L = L_0 + \delta^{\alpha} L_1, \tag{5.6}$$

where L_0 is the lubrication result. The exponent α can be estimated by the following scaling argument. From lubrication analysis of flow through the gap between a plane and a circular cylinder, the length along the gap over which the stresses act is $O(\sqrt{ah_0})$, and the viscous stresses are $O(\mu\Omega a/h_0)$. Outside the gap, the length over which the stresses act is $O(a)$ and the stresses have magnitude $O(\mu\Omega)$. Since the torque per unit width is stress times moment arm a, times the length over which they act, the ratio of the net torque outside the gap to the torque inside is

$$\frac{\text{net torque/width outside gap}}{\text{net torque/width inside gap}} = \frac{\mu\Omega a^2}{(\mu\Omega a^2/h_0)\sqrt{ah_0}} = \sqrt{\frac{h_0}{a}} = \delta^{1/2}. \tag{5.7}$$

Therefore the second-order correction term in an approximation for the torque should be $O(\delta^{1/2})$ as shown in figure 15(*b*) and $L_1 \approx 28.6$. However, to incorporate this outer problem into the lubrication analysis would require matching the inner problem to the outer region which appears to be complicated given the non-trivial geometry, and is not attempted here. It will be sufficient for our purposes to observe that the torque begins to tend toward the lubrication approximation when $\delta \leqslant 0.5$, for $\eta = 1/2$.

6. Conclusions

We have used the lubrication approximation to show that the general solution for the flow over a rotating cylinder eccentrically placed in a two-dimensional channel can be found in terms of four flow parameters q, Ω, Δp, and L, and two geometrical parameters η and δ. There are four equations, each of which linearly relates three of the four flow parameters. Given two flow parameters, the optimal geometry η or δ can be found in order to optimize a third parameter. For example, the optimization allows a designer of MEMS devices to calculate the critical gap sizes for a particular desired quantity, such as maximum flow rate. Also, it is shown that a device of this configuration cannot be developed that achieves maximum flow rate and rotation simultaneously, even for non-zero applied torque. Boundary integral methods are demonstrated to be suitable for this problem where resolution in the thin gaps is important. This numerical solution is shown to approach the lubrication limit for the case of zero rotation, and the relative difference is approximately 2% for $\delta = 0.1$, where the sum of the gaps is 10% of the radius of the cylinder. For non-zero rotation and non-zero torque, $\Delta\hat{p}$ from the boundary integral solution is shown to approach the lubrication solution to within 5% when $\delta = 0.5$ and to within 1% when $\delta = 0.1$. The result for torque approaches the lubrication solution more slowly, reaching 10% difference when $\delta = 0.05$ for $\eta = 1/2$. The second-order correction term for the lubrication approximation of torque is shown to be proportional to $\delta^{1/2}$.

The authors are grateful for support by a research grant from the Army Research Office (DAAG55-97-1-0114). The authors thank Roger Brockett for helpful conversations.

REFERENCES

Aluru, N. R., Lin, L., Forster, F. K. & Zhang, X. (Eds.) 1998 *Micro-Electro-Mechanical Systems* (*MEMS*). DSC, Vol. 66. ASME.

Batchelor, G. K. 1967 *An Introduction to Fluid Dynamics*. Cambridge University Press.

DeCourtye, D., Sen, M. & Gad-el-Hak, M. 1998 Analysis of viscous micropumps and microturbines. *Intl J. Comput. Fluid Dyn.* **10**, 13–25.

Ho, C.-M. & Tai, Y.-C. 1998 Micro-electro-mechanical systems (MEMS) and fluid flows. *Ann. Rev. Fluid Mech.* **30**, 579–612.

Keller, J. B. 1964 Viscous flow through a grating or lattice of cylinders. *J. Fluid Mech.* **18**, 94–96.

Kim, S. & Karrila, S. J. 1991 *Microhydrodynamics: Principles and Selected Applications*. Butterworth–Heinemann.

Leal, L. G. 1993 *Laminar Flow and Convective Transport Processes: Scaling Principles and Asymptotic Analysis*. Butterworth–Heinemann.

Pozrikidis, C. 1992 *Boundary Integral and Singularity Methods for Linearized Viscous Flow*. Cambridge University Press.

Sen, M., Wajerski, D. & Gad-el-Hak, M. 1996 A novel pump for MEMS applications. *Trans. ASME: J. Fluids Engng* **118**, 624–627.

Sharatchandra, M. C., Sen, M. & Gad-el-Hak, M. 1997 Navier–Stokes simulations of a novel viscous pump. *Trans. ASME. J. Fluids Engng* **119**, 372–382.

Tanzosh, J., Manga, M. & Stone, H. A. 1992 Boundary integral methods for viscous free-boundary problems: Deformation of single and multiple fluid–fluid interfaces. In *Proc. Boundary Element Technologies VIII* (ed. C. A. Brebbia & M. S. Ingber), pp. 19–39. Computational Mechanics Publications.

Wenning, S. (Ed.) 1999 *Technical Proc. Second Intl. Conf. on Modeling and Simulation of Microsystems*. Computational Publication, San Juan, Puerto Rico.

Youngren, G. K. & Acrivos, A. 1975 Stokes flow past an arbitrary particle. *J. Fluid Mech.* **69**, 382–383.